26. L. Y. Chen and N. C. MacDonald, *Digest IEEE Int. Conf. Solid-State Sensors Actuators* (June 1991), p. 739.
27. Z. L. Zhang and N. C. MacDonald, *ibid.*, p. 520.
28. Y. Gianchandani and K. Najafi, *Digest IEEE Int. Electron Devices Meeting* (December 1991), in press.
29. K. Suzuki, *ibid.*, p. 625.
30. W. Ehrfeld, F. Gotz, D. Munchmeyer, W. Schelb, D. Schmidt, *Digest IEEE Solid-State Sensor Actuator Workshop* (June 1988), p. 1.
31. H. Guckel *et al.*, *Digest IEEE Solid-State Sensor Actuator Workshop* (June 1990), p. 118.
32. H. Guckel *et al.*, *Digest IEEE Int. Conf. Solid-State Sensors Actuators* (June 1991).
33. Y. W. Kim and M. G. Allen, *ibid.*, p. 651.
34. R. M. Harris, F. Maseeh, S. D. Senturia, *Digest IEEE Solid-State Sensor Workshop* (June 1990), p. 36.
35. Y. Zhang, S. B. Crary, K. D. Wise, *ibid.*, p. 32.
36. H. H. Zappe, *Digest IEEE MicroElectroMechanical Systems* (February 1990).
37. C. F. Quate, *ibid.*, p. 188.
38. L. C. Kong, B. G. Orr, K. D. Wise, *Digest 1990 IEEE Solid-State Sensor Actuator Workshop* (June 1990), p. 28.
39. We acknowledge the many efforts of those at the University of Michigan who have contributed to the work described in this article. In particular, we thank J. Ji, S. Cho, E. Yoon, S. Crary, B. G. Orr, J. F. Hetke, L. C. Kong, N. Najafi, A. C. Hoogerwerf, Y. Gianchandani, and the staff of the Solid-State Fabrication Facility. The support and assistance of F. T. Hambrecht and W. Heetderks of the Neural Prosthesis Program, National Institute of Neurological Disorders and Stroke, R. M. Burger and N. Foster of the Semiconductor Research Corporation, and G. Hazelrigg of the National Science Foundation have made our particular activities at the University of Michigan possible.

Research Article

Three-Dimensional Structures of the Ligand-Binding Domain of the Bacterial Aspartate Receptor With and Without a Ligand

MICHAEL V. MILBURN,* GILBERT G. PRIVÉ,† DANIEL L. MILLIGAN,‡ WILLIAM G. SCOTT, JOANNE YEH, JARMILA JANCARIK, DANIEL E. KOSHLAND, JR.,§ SUNG-HOU KIM§

The three-dimensional structure of an active, disulfide cross-linked dimer of the ligand-binding domain of the *Salmonella typhimurium* aspartate receptor and that of an aspartate complex have been determined by x-ray crystallographic methods at 2.4 and 2.0 angstrom (Å) resolution, respectively. A single subunit is a four–α-helix bundle with two long amino-terminal and carboxyl-terminal helices and two shorter helices that form a cylinder 20 Å in diameter and more than 70 Å long. The two subunits in the disulfide-bonded dimer are related by a crystallographic twofold axis in the apo structure, but by a noncrystallographic twofold axis in the aspartate complex structure. The latter structure reveals that the ligand binding site is located more than 60 Å from the presumed membrane surface and is at the interface of the two subunits. Aspartate binds between two α helices from one subunit and one α helix from the other in a highly charged pocket formed by three arginines. The comparison of the apo and aspartate complex structures shows only small structural changes in the individual subunits, except for one loop region that is disordered, but the subunits appear to change orientation relative to each other. The structures of the two forms of this protein provide a step toward understanding the mechanisms of transmembrane signaling.

TRANSMEMBRANE RECEPTORS ARE THE PROTEINS THROUGH which cells and organisms commonly receive information from the outside of a cell and transmit it for processing inside the cell. One type of receptor is connected to an ion channel and allows a burst of ions to enter or leave the cell, but in most cases the receptor information is probably transferred from exterior to interior through conformational changes in the protein. The mechanism of information transfer is obscure, in part because it has been difficult to crystallize any transmembrane receptor. Although two membrane proteins, a photoreaction center (*1*) and a porin (*2*), have been crystallized and their crystal structures have been determined, they do not have the structure of a typical receptor of signal transduction. For one such class, of which the epidermal growth factor (*3*), platelet-derived growth factor (*4*), insulin (*5*), and low-density lipoprotein (*6*) receptors are typical, the proteins contain an extracellular ligand-binding domain, a cytoplasmic signaling domain, and a transmembrane domain composed of one or two transmembrane hydrophobic sequences. The aspartate receptor of chemotaxis falls in this last category (*7*) and is itself a member of a large family of bacterial protein receptors (*8*). The ligand-binding domain of the aspartate receptor has been crystallized in the presence and absence of aspartate. Structural properties have been revealed that represent an initial step toward unraveling the mechanism of transmembrane signaling in this and other related receptors.

The aspartate receptor of *Salmonella typhimurium* has been extensively studied, and the features of its primary structure are summa-

M. V. Milburn, G. G. Privé, W. G. Scott, J. Yeh, J. Jancarik, and S.-H. Kim are in the Department of Chemistry and Lawrence Berkeley Laboratory, University of California, Berkeley, CA 94720. D. L. Milligan and D. E. Koshland, Jr., are in the Department of Biochemistry, University of California, Berkeley, CA 94720.

*Present address: Department of Structural and Biophysical Chemistry, Glaxo Inc., Research Triangle Park, NC 27790.
†Present address: Molecular Biology Institute, University of California, Los Angeles, CA 90024.
‡Present address: Howard Hughes Medical Institute, University of California, San Francisco, CA 94143.
§To whom correspondence should be addressed.

rized below. The exterior periplasmic domain (residues 31 to 188) contains the aspartate binding site and is connected to the interior cytoplasmic domain (residues 1 to 6 and 213 to 552) by two transmembrane sequences (residues 7 to 30 and 189 to 212) (*7, 8*). Genetic and biochemical evidence has indicated that Arg^{64}, Arg^{69}, Arg^{73} (*9*), and Thr^{154} (*10*) are involved in aspartate binding or signal transmission and that Glu^{295}, Glu^{302}, Glu^{309}, and Glu^{491} are sites of covalent modification during the signaling process (*11*). The biochemistry of transmembrane receptor–mediated chemotaxis and regulation through covalent modification has been thoroughly reviewed (*12*). A cloned fragment of the amino-terminal domain (residues 26 to 188) is water soluble and binds aspartate with wild-type affinity (*13*). We report the major features of the crystal structures of an active, disulfide-linked dimer of the ligand domain of the aspartate receptor in the presence and absence of aspartate and discuss the implications of the structural differences on signal transduction of this transmembrane receptor.

Protein preparation and crystallization. Although the detailed procedures for preparation and crystallization of the ligand-binding domain of the aspartate receptor have been reported (*14*), the essentials are briefly summarized as follows. The ligand-binding domain (beginning with Met^{25} and ending with Arg^{188}) was produced from a multicopy plasmid and exported to the periplasm, extracted by mild osmotic lysis, precipitated by ammonium sulfate, and purified to homogeneity by anion exchange and other chromatographic methods. The purified protein exists primarily as a dimer and binds aspartate with essentially wild-type affinity. Because crystals of the wild-type protein diffracted poorly, a functionally active disulfide-linked dimer of the ligand-binding domain containing Cys at position 36 was crystallized and used for high-resolution studies. The corresponding intact receptor dimer containing a Cys^{36} cross-link has been shown to signal in the same way as the wild-type receptor, although this cross-linked receptor appears to be somewhat activated when compared to the wild-type receptor (*15*).

Crystal structure determination. The native crystals of the apo and aspartate complex proteins diffract to beyond 2.2 and 2.0 Å resolution, respectively (*16*). Complete data sets of the native crystals, as well as data for a $KAu(CN)_2$ and $K_2Hg(SCN)_4$ isomorphic derivative of the apo protein crystals, were collected and processed (*17–20*). Difference Patterson maps revealed two heavy-atom sites for each derivative, and the Au sites were independently confirmed in an anomalous Patterson map (*21*). Multiple isomorphous replacement (MIR) with anomalous scattering phase refinement was carried out in the space group $P6_522$ with the program package PROTEIN (*20*) with data between 10.0 and 3.0 Å resolution. The phasing power of the Au data was 1.93 and that of the Hg data was 0.95. The average figure of merit for the phase determination was 0.60. The MIR phase set was then solvent-flattened (*22*), and phases were extended to 2.7 Å resolution with the calculated molecular envelope of the protein at 3.0 Å resolution.

The resulting electron density map revealed (Fig. 1A) a cluster of four roughly parallel α helices (Fig. 2), and the handedness of these helices confirmed the space group to be $P6_522$ rather than $P6_122$. Two of the helices were parallel to one another and antiparallel to the two others, thus restricting the possible connectivities within the protein. The chain tracing was verified by several marker features, including: (i) the location of the Cys^{36} disulfide cross-link joining the two crystallographic symmetry-related subunits; (ii) the location of Trp^{57} as well as many other aromatic side chains including Phe^{40}, Phe^{107}, Phe^{140}, Phe^{180}, Tyr^{104}, Tyr^{127}, and Tyr^{130}; and (iii) most amino acid residues at the binding sites of the heavy atoms (glutamines and glutamates) having the functional groups compatible for metal coordination—three of the four heavy atoms bind at the interface of the crystallographic dimer.

A total of 154 amino acids were assigned to the electron density, starting with Met^{25} and ending at Phe^{180}. The eight carboxyl-terminal amino acids could not be assigned to the electron density; presumably they are disordered. This initial structure was refined with a slow-cooling simulated annealing method with the program XPLOR 2.1 (*23*). Data from 8.0 to 2.4 Å resolution were used with a temperature decrease from 4000 to 300 K with 50 cycles of refinement at 0.5-fs steps for each 25 K decrease in temperature. An

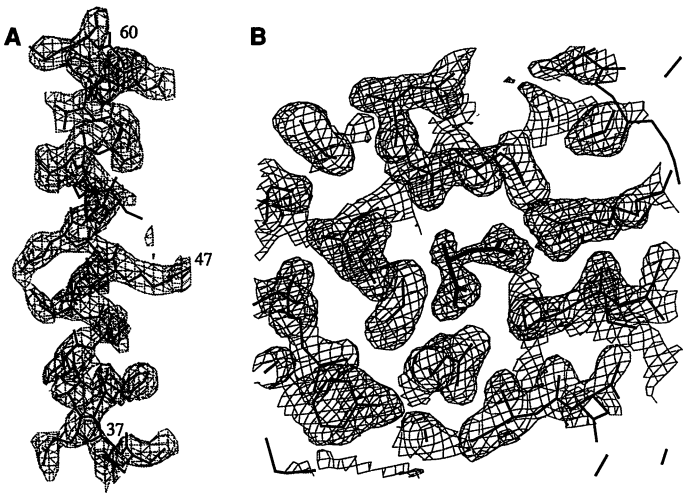

Fig. 1. (**A**) Residues 37 through 60 are plotted with the electron density from the solvent flattened map calculated with 2.7 Å resolution data of the apo crystal, contoured at 1σ of the map root-mean-square (rms). Based on this map, most of the residues could be easily identified to the protein sequence including those with branched side chains. Most notable among those that are plotted is: (i) Cys^{36} at the bottom of the figure, which formed a continuous piece of density across the twofold axis to the other cross-linked subunit; (ii) Arg^{47}, Leu^{53}, and Thr^{56} toward the top of the figure that, even at 2.7 Å resolution, clearly showed the branching of the side chains; and (iii) Trp^{57} at the top of the figure, which was identified early on in the protein tracing. (**B**) Electron density of aspartate; $2F_o - F_c$ electron density of the aspartate complex crystal calculated before the aspartate ligand was included in the refinement model. The contour level is 1.0σ. The model shown is based on the current refinement with the aspartate shown in thick lines and the protein atoms in the ligand pocket in lighter lines.

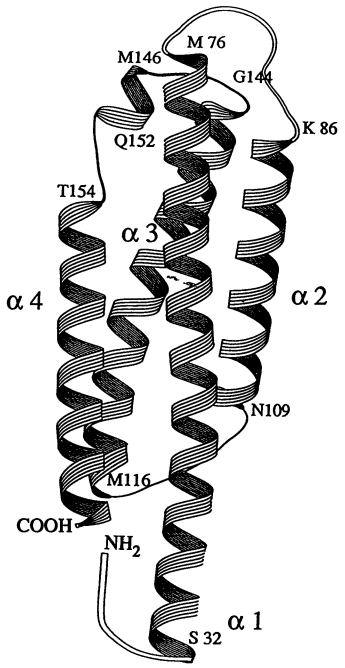

Fig. 2. Ribbon drawing (*41*) of the ligand-binding domain of the aspartate receptor from *Salmonella typhimurium*. The beginning and ending residues of each α helix are labeled, as was determined by visual inspection of the MIR map and by using the secondary structure identification program DSSP (*42, 43*). The subunit has the prolate shape with a length of ~70 Å and a diameter of 20 Å. Residues 25 to 31, which are a part of the first transmembrane region, are nonhelical in our structure, but this is probably an artifact due to the absence of membrane in the crystals. The last ordered residue at the carboxyl (C) terminus in our electron density maps is residue 180, which is at the end of helix α4.

R factor of 0.27 was obtained with an overall temperature factor of 20.0 Å^2 for all atoms. Refinement was continued with several cycles of refinement and manual refitting of the protein to the density. Apart from the eight carboxyl-terminal residues, one loop region in the model from residue Asn^{80} to Lys^{86} corresponds to the weakest electron density in the map and consequently these residues have the highest temperature factors.

The structure of the complex between the protein and aspartate was solved by molecular replacement by Patterson correlation refinement (*23*) using a subunit from the unliganded structure as a probe model. (Residues 25 to 34 and 76 to 86, corresponding to the amino terminal and the first loop regions of the apo model, respectively, were not included in the search model.) Two independent and unambiguous solutions were found that correspond to a Cys^{36} cross-linked dimer in the asymmetric unit. The initial crystallographic *R* factor for this solution before any refinement was 0.368 for the 5836 reflections between 8 to 3 Å resolution with a single overall temperature factor. Refinement with conjugent gradient minimization reduced the *R* factor to 0.246 for a 6 to 2.5 Å data set containing 8569 reflections with a single overall *B* factor. Data to 2.0 Å were then included, positions were refined with simulated annealing minimization (*23*), and atomic temperature factors were refined. A single aspartate ligand was identified and built into the resultant electron density map (Fig. 1B), as well as residues 25 to 34 and 76 to 86, which were absent in the search model. Solvent peaks are clear in the current electron density maps, but no water molecules have yet been included in the crystallographic refinement except those in the ligand-binding pocket.

Backbone structure. The three-dimensional backbone structure of the ligand-binding domain subunit of the aspartate receptor is a four-helix bundle (*24*) as shown in Fig. 2, which also identifies the beginning and ending residues of each helix. Similar helix bundles have been observed in hemerythrin (*25*), apoferritin (*26*), and the receptor-binding domain of apolipoprotein E (*27*). The first long helix spans the length of the periplasmic domain from residue 32 to 76, yielding a continuous 12-turn helix with 45 amino acids. Although we describe the structure as a four–α-helix bundle, the carboxyl-terminal helix is split into two: one helix has two turns and one helix has six turns (Fig. 2). The crystal structure has overall features similar to a model of this receptor that was based on optical rotary dispersion, biochemical data, and secondary structure predictions (*28*), although the detailed features are different. Perhaps the most striking feature of the overall protein structure is the extreme prolate shape of the molecule. The longest dimension of the molecule, the axis of the helix bundle, is more than 70 Å, whereas the diameter is ~20 Å. Although primarily composed of different secondary structures, the CD4 receptor ligand domain of T lymphocytes (*29*) and the influenza virus particle surface protein hemagglutinin (*30*) have a similar prolate shape, suggesting that this overall morphology may well be typical of the external domains of many other transmembrane proteins.

The functional form of the aspartate receptor ligand-binding domain is a dimer. Each subunit contains a four–α-helical bundle arranged in parallel to form a cluster of eight helices (Fig. 3). The monomer subunits, named A and B, are composed of helices α1-α4 and α1′-α4′, respectively. In the apo structure they are related by an exact crystallographic twofold axis that runs along the long dimension of the molecule near the two amino-terminal helices, which results in a close association between helices α1 and α1 . With α4 and α4′ nearby, these four helices form a "quasi"–four-helix bundle in the core of the dimer, in that it is less compact than a regular four-helix bundle and is composed of two different peptides, that is, α1 and α4 from one subunit and α1′ and α4′ from the other (Fig. 3). The dimer interface has two contacting regions, one on top and the other at the bottom of Fig. 3, with a 6 Å wide channel across the middle of the dimer that is wide enough to allow the passage of water and other small molecules between the subunits.

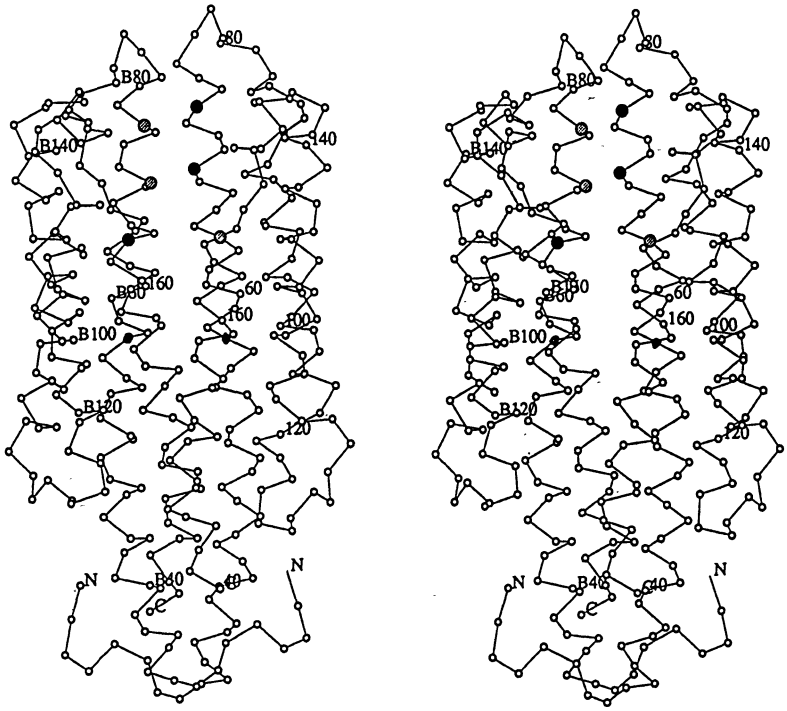

Fig. 3. Stereo view of the Cα atoms in the apo form of the disulfide-linked ligand-binding dimer; Arg^{64}, Arg^{69}, and Arg^{73}, which are implicated genetically in ligand binding, are shown as shaded and enlarged circles. The twofold axis that relates the two subunits is vertical in the plane of the page, between the two central amino-terminal helices. Note that residues 64 and 154 of one subunit and residues 69 and 73 of the other (shown in black) form a pocket.

Ligand-binding pockets. The molecular symmetry generates two ligand-binding sites, each at the dimer interface within the quasi–four-helix bundle near the top of the molecule, distal from the membrane (Fig. 3). Of the two ligand-binding sites, one is fully occupied and shows clear electron density for an aspartate (Fig. 1B), whereas the second shows weaker density that may be due to a disordered aspartate or a sulfate ion, which is present in high concentration in the crystals. The binding stoichiometry is thought to be one aspartate per receptor subunit (*31*), but preliminary experiments indicate that aspartate binding to the receptor fragment is substantially weaker in solutions containing high Li_2SO_4 concentrations (*32*), and our crystallization solutions apparently did not contain enough aspartate to fully saturate both sites of the protein.

The detailed interactions between aspartate and the residues in the ligand pocket are shown in Fig. 4. Each binding pocket is formed by Arg^{64} and residues 149 to 154 from one subunit and by Arg^{69} and Arg^{73} from the other subunit. The two aspartate carboxylate groups form hydrogen bonds with three positively charged arginines: Arg^{64} (molecule A) forms two bonds to the α-carboxyl; Arg$^{69'}$ (molecule B) interacts with both the α- and γ-carboxyls; and Arg$^{73'}$ (molecule B) makes two bonds to the γ-carboxyl. The aspartate amino group is tightly bound in the pocket formed by the main-chain carbonyls of Tyr^{149} and Gln^{152} and the side-chain hydroxyl group of Thr^{154}. The three electronegative oxygens all point toward the aspartate NH_3^+ group, and the

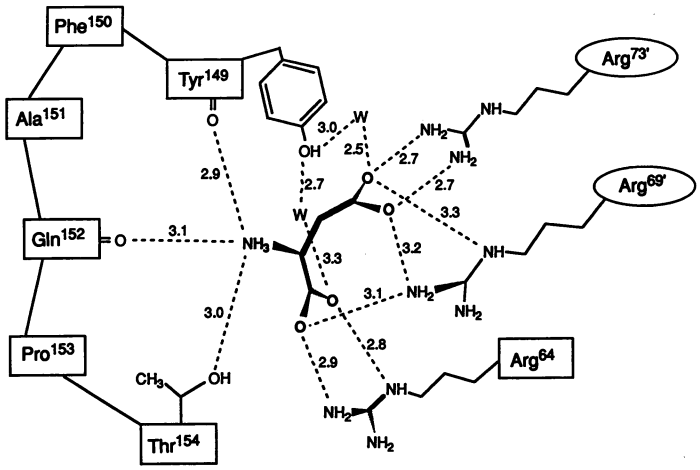

Fig. 4. Drawing of the hydrogen-bonding interaction scheme at the aspartate binding site. The boxed amino acids are from subunit A, and those in ovals are from subunit B. The two waters are labeled "W." Presumed hydrogen bonds are in dashed lines with corresponding distances.

formation of this amino-binding pocket is determined largely by the presence of Pro^{153}, which causes a local disruption in helix α4. A hydrophobic interaction between the aspartate methylene group and the aromatic ring of Tyr^{149} completes the direct interactions between the protein and the ligand. Genetic and biochemical studies have shown that Thr^{154} (*10, 33*) and Arg^{64}, Arg^{69}, and Arg^{73} (*9*) are all important for aspartate binding, and the structural basis for their importance is evident in the crystal structure. There are several water-mediated interactions between the aspartate and protein residues on molecule A. Four water molecules are bound directly to the aspartate carboxyls, two of which are involved in bridges between the aspartate and the protein (Fig. 4). One of these waters links an aspartate γ-carboxyl oxygen to both the hydroxyl of Tyr^{149} and to the side chain of Ser^{68}, and the other water forms hydrogen bonds with the aspartate α-carboxyl, the Tyr^{149} hydroxyl, and the main-chain carbonyl of Arg^{64}.

The aspartate is buried deep at the dimer interface, with 80 percent of its accessible surface area buried within the protein. Of this area, 40 percent is in contact with molecule B (mostly with the two carboxyl groups) and 60 percent with molecule A (involving salt linkages with the α-carboxyl and α-amino groups and van der Waals interactions with Cα and Cβ). As described above, more residues from molecule A are involved in the aspartate-binding pocket than residues from molecule B.

In addition to the aspartate ligand site, a separate binding site for an aromatic compound has been located at the interface between the two receptor subunits. The density assigned to a phenanthroline molecule (present in crystallization) is located on the twofold axis in the lower part of the dimer, and this molecule is tightly packed between the side chains of the aromatic amino acids Phe^{30}, Phe^{40}, Tyr^{176}, and Phe^{180} from each subunit half. This binding site might be biologically important for sensing small aromatic ligands such as phenol. There is evidence that phenol induces chemotaxis in *Escherichia coli* and *S. typhimurium* (*34*), but it is not clear at the present time if phenol is the natural ligand for this pocket.

Conformational changes upon ligand binding. A least-squares fit of the Cα atoms between the single apo subunit and each of the two subunits of the aspartate complexed dimer reveals only small changes in the apo and aspartate complex of the protein, except for loop L1 (residues 77 to 85), which is in a different packing environment in the apo and complex crystals, and the "amino pocket" (residues 149 to 154). The root-mean-square (rms) deviation between Cα atoms of an individual apo subunit and subunit A of the complex structure is only 0.47 Å, excluding residues 25 to 36 at the amino terminus, the loop L1 region, the amino pocket, and two residues from loop L2 that are affected by a packing contact. The equivalent deviation between an apo subunit and the B subunit is 0.34 Å, with a good fit even for loop L2 and the amino pocket in this case. Thus, apart from the flexible loop L1 and the slight internal reorganization of the ligand binding region, the individual subunits remain largely unaffected by aspartate binding, including the relative positions of α1 and α4, which are connected to two transmembrane domains. However, when one subunit of the apo structure is superimposed onto a subunit of the complex structure, the rms deviation between two remaining subunits is 1.4 Å, indicating that the shift of subunits relative to one another is the primary conformational change of the dimer upon ligand binding. The simplest description of the conformational change is a 4° rotation between the subunits about a pivot axis that is roughly perpendicular to both the dimer interface and the dimer twofold axis, and thus parallel to the presumed membrane surface. There are three interpretations for the observation: This relatively small rotation (i) could be an artifact due to two different crystal packing environments or (ii) could represent a much larger conformational change that is possibly dampened due to the Cys^{36} disulfide bond between the two subunits or crystal lattice forces or (iii) is an actual change that could be amplified more than 100 Å away at the cytoplasmic domains.

The effect of aspartate binding is to bring the binding-pocket residues from both subunits closer together. Aspartate locks the dimer into a tighter complex by both the gain of favorable (attractive) interactions between the aspartate and the protein and loss of

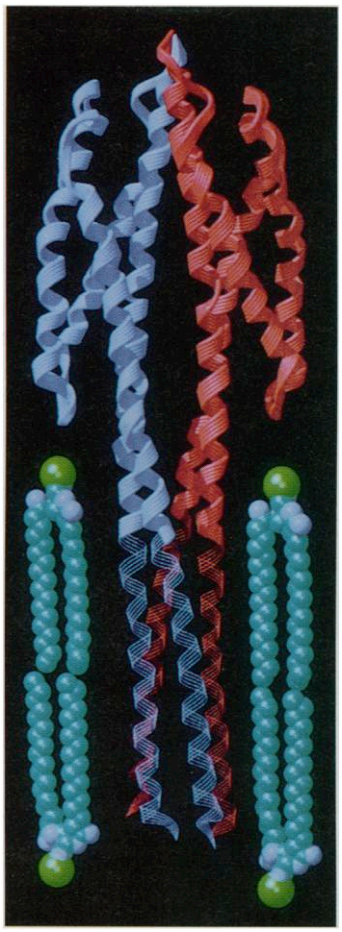

Fig. 5. Ribbon drawing (*41*) of the dimer including the modeled transmembrane region (shown in thin ribbons) as it may be in the cell. The lipid molecules are placed according to the beginning and ending of protein hydrophobic residues believed to traverse the membrane. The model for the dimer is >120 Å long and ~40 Å in diameter.

Table 1. Refinement results. Refinement statistics for the apo and aspartate complex of the ligand-binding domain of the aspartate receptor. After XPLOR (*23*) simulated annealing refinement, the structure was further refined with 100 rounds of TNT refinement (*40*). The results presented here are for the structure with no added water molecules (except for four waters in the ligand pocket of the complex structure) or phenanthroline.

Parameter	Apo	Complex
Maximum resolution (Å)	2.4	2.0
Unique reflections (no.)	12,236	19,191
Total number of observations ($I > \sigma$)	62,891	78,886
R_{merge}	0.0684	0.069
Completeness of data	0.972	0.821
R factor (no waters included)	0.204	0.216*
Total number of non-hydrogen atoms	2,462	2,471
Average temperature factor (all atoms) (Å^2)	23.5	25.1
Rms bond deviation from ideal (Å)	0.019	0.014
Rms angle deviation from ideal (degrees)	2.4	2.9
Rms dihedral deviation from ideal (degrees)	25.1	20.4

*Four waters at the aspartate binding site are included.

unfavorable (repulsive) electrostatic interactions among arginines. This effect explains the observation that addition of aspartate decreases the rate of dissociation and exchange of subunits in the intact receptor dimer (*35*).

A model for the transmembrane domain. The putative membrane-spanning regions of the protein sequence (residues 7 to 30 and 189 to 212) are substantially hydrophobic in character and are predicted to form two α helices (*7*), which we have modeled to continue uninterrupted from the amino- and carboxyl-terminal long helices (α1 and α4 in Fig. 2) of the ligand domain structure. The attached transmembrane helices were then energy-minimized in XPLOR 2.1 (*23*) to reduce sterically unfavorable side-chain contacts and to optimize protein dimer interactions. The resulting model of the aspartate-binding domain dimer with attached membrane-spanning helices is shown in Fig. 5. In the model, four α helices, two from each subunit, form a long quasi–four-helix bundle and connect the ligand binding region and the cytoplasmic domain, which are separated by a distance of more than 100 Å.

A continuous helical structure has been indicated by a cysteine cross-linking study (*36*) which has shown that residues 18 and 19 in the first transmembrane region (TM1) are close in space to positions 18′ and 19′ on the alternate subunit, whereas residues 198 to 201 in the second transmembrane domain (TM2) are distant from their 198′ to 201′ counterparts. In the quasi–four-helix model of the transmembrane domain described above, the residues 18 and 18′ are closely juxtaposed, whereas residues 198 to 201 are distant, which supports the assumption that α1 and α1′ continue through the membrane as relatively uninterrupted helices and suggests that the 36-36′ cross-link does not adversely affect the structure.

Structural implications for signal transduction. The structural features described in this article may have important implications for the mechanism of transmembrane signal generation. The helices of the quasi–four-helix bundle in the central core of the dimer (α1, α4, α1′, and α4′) are the key to the signaling mechanism since they continue through the membrane (*36*), and the binding of aspartate must affect these helices over a distance exceeding 120 Å from the ligand-binding site at the top of the receptor down to the cytoplasmic domain. Three general, limiting-case models for transmembrane signaling in this receptor can be considered. Aspartate binding causes: (i) an internal change within a subunit, so that relative changes between α1 and α4 are sensed in the cytoplasmic domain [recent studies with truncated receptors (*37*) give support for such an effect]; (ii) a change between the subunits with a possible "scissor-type" motion in the intersubunit orientations as suggested by the crystallographic studies described in this article; or (iii) a combination of the above intra- and intersubunit motions.

These questions still need to be tested, but our study indicates that: (i) the ligand binding site for a transmembrane receptor can be far away from the membrane (more than 60 Å from the surface); (ii) continuous α helices more than 120 Å long appear to stretch from the ligand-binding site, which is the point of signal generation, down to the point of signal action in the cytoplasm; and (iii) the conformational changes caused by the ligand binding at the dimer interface suggest a realignment of the helices at the interface relative to each other, thus transmitting conformational information from the periplasm to the cytoplasm. The small changes that are observed suggest that the lack of transmembrane domain, the S-S cross-links, or the crystal lattice forces may tilt the protein partially to the aspartate-bound form, dampening an otherwise larger conformation change on aspartate binding.

It is intriguing that many mammalian transmembrane receptors such as the epidermal growth factor receptor are postulated to be activated by an association mechanism (*38*). Although significant differences exist between this class of receptors and the aspartate receptor, the former having one transmembrane and the latter two per subunit, both do feature an association of subunits, and a realignment of helices relative to each other might be a common feature of both classes of receptor. The fact that a chimera of the ligand and transmembrane domain of the aspartate receptor and the cytoplasmic domain of the insulin receptor, which also contains two transmembrane helices, can transduce a signal (*39*), is further indication that there may be common mechanisms of signal transduction in many different types of receptors.

REFERENCES AND NOTES

1. J. Deisenhofer *et al.*, *J. Mol. Biol.* **180**, 385 (1984); J. P. Allen *et al.*, *Proc. Natl. Acad. Sci. U.S.A.* **84**, 5370 (1987).
2. M. S. Weiss *et al.*, *FEBS Lett.* **280**, 379 (1991).
3. A. Ullrich *et al.*, *Nature* **309**, 418 (1984).
4. L. Claesson-Welsh *et al.*, *Mol. Cell Biol.* **8**, 3476 (1988).
5. Y. Ebina *et al.*, *Cell* **40**, 747 (1985).
6. T. Yamamoto *et al.*, *ibid.* **33**, 615 (1984).
7. A. F. Russo and D. E. Koshland, Jr., *Science* **220**, 1016 (1983).
8. A. Krikos, N. Mutoh, A. Boyd, M. I. Simon, *Cell* **33**, 615 (1983).
9. C. Wolff and J. S. Parkinson, *J. Bacteriol.* **170**, 4509 (1988); S. L. Mowbray, D. E. Koshland, Jr., *J. Biol. Chem.* **265**, 15638 (1990).
10. L. Lee and Y. Imae, *J. Bacteriol.* **172**, 377 (1990).
11. T. Terwilliger, J. Y. Wang, D. E. Koshland, Jr., *Proc. Natl. Acad. Sci. U.S.A.* **83**, 6707 (1986).
12. D. E. Koshland, Jr., *Biochemistry* **27**, 5829 (1988); R. B. Bourret, J. F. Hess, K. A. Borkovich, A. A. Pakula, M. I. Simon, *J. Biol. Chem.* **264**, 7085 (1989); J. B. Stock, A. M. Stock, J. M. Mottonen, *Nature* **344**, 395 (1990).
13. D. L. Milligan and D. E. Koshland, Jr., unpublished results.
14. J. Jancarik, W. G. Scott, D. L. Milligan, D. E. Koshland, Jr., S.-H. Kim, *J. Mol. Biol.* **221**, 31 (1991).
15. F. J. Falke and D. E. Koshland, Jr., *Science* **237**, 1596 (1987); D. L. Milligan and D. E. Koshland, Jr., *J. Biol. Chem.* **263**, 6268 (1988).
16. High-quality single crystals of the ligand-binding domain in the absence of aspartate were obtained by the sitting drop technique from solutions containing 10 mg/ml protein, 0.05 M Hepes buffer at pH 7.4, 0.75 M Li_2SO_4, and 0.5 mM Cu(II)[1,10-phenanthroline]$_3$ (added to maintain the disulfide cross-link), and equilibrated against 0.1 M Hepes and 1.5 M Li_2SO_4 at the same pH at 21°C. The space group of the crystals is $P6_522$ with cell dimensions $a = b = 80.03$ Å and $c = 155.6$ Å. One half of the Cys^{36} cross-linked dimer of the periplasmic domain resides in an asymmetric unit. The sparse matrix method [J. Jancarik and S.-H. Kim, *J. Appl. Crystallogr.* **24**, 409 (1991)] was used for screening crystallization conditions. Crystals of the periplasmic domain complexed with aspartate were grown under the same conditions except that the crystallization solution contained 2 mM aspartate. The complex protein crystallized in space group $P3_221$ with unit cell dimensions $a = b = 80.38$ Å and $c = 91.35$ Å.
17. Complete data sets of the native crystals as well as data for $KAu(CN)_2$ isomorphic derivative of the apo protein were collected on phosphor imaging plates with a specially designed Weissenberg camera [N. Sakabe, *J. Appl. Crystallogr.* **16**, 542 (1983)] on synchroton x-ray at Photon Factory, Tsukuba, Japan, or an R-AXIS-II camera made by Rigaku, Japan. The digitized images were reduced to structure factor amplitudes with the program WEIS (*18*). Data for the $K_2Hg(SCN)_4$ isomorphic derivative of the apo protein were collected on x-ray film at a wavelength of 1.54 Å with an Enraf-Nonius rotation camera at the Stanford

Synchrotron Radiation Laboratory. The films were digitized with a drum scanner (Optronix Corp.), and the data were processed with computer programs originally written by Rossmann (*19*). The native and the Hg data were merged and scaled with the crystallographic program package PROTEIN (*20*), and the Au data were merged and scaled for anomalous scattering data with programs from the CCP4 package. [S.E.R.K. (U.K.) Collaborative Computing Project No. 4 (Daresbury Laboratory, Warrington, U.K., 1979)].
18. T. Higashi, *J. Appl. Crystallogr.* **22**, 9 (1989).
19. M. G. Rossmann, *ibid.* **12**, 225 (1979).
20. W. Steigemann, *PROTEIN: A Package of Crystallographic Programs for Analysis of Proteins* (Max Planck Institute for Biochemistry, Martinsried, Germany, 1982).
21. In order to determine the correct space group enantiomorph, phases from the Au derivative anomalous scattering data were calculated in the space groups $P6_122$ and $P6_522$ and tested in difference ($F_{Hg} - F_{nat}$) Fourier syntheses. The two Hg sites emerged as the two strongest peaks in the electron density maps when the data were treated in the space group $P6_522$, whereas the map calculated in $P6_122$ had much weaker Hg peaks, thus confirming the former as the correct space group.
22. B. C. Wang, *Methods Enzymol.* **115**, 90 (1985).
23. A. T. Brünger, *X-PLOR Version 2.1* (Yale University, New Haven, CT, 1990).
24. P. Argos, M. G. Rossmann, J. E. Johnson, *Biochem. Biophys. Res. Commun.* **75**, 83 (1977).
25. K. B. Wark, W. A. Hendrickson, G. L. Klippenstein *Nature* **257**, 818 (1975).
26. S. H. Banyard, D. K. Stammers, P. M. Harrison, *ibid.* **271**, 282 (1978).
27. D. R. Breiter *et al.*, *Biochemistry* **30**, 603 (1991); C. Wilson *et al.*, *Science* **252**, 1817 (1991).
28. G. R. Moe and D. E. Koshland, Jr., in *Microbial Energy Transduction: Genetics, Structure and Function of Membrane Proteins*, D. C. Youvan and F. Daldal, Eds. (Cold Spring Harbor Laboratory, Cold Spring Harbor, NY, 1986), pp. 163–168.
29. J. H. Wang *et al.*, *Nature* **348**, 411 (1990); S. E. Ryu *et al.*, *ibid.*, p. 419.
30. I. A. Wilson, J. J. Skehel, D. C. Wiley, *ibid.* **289**, 368 (1981); D. C. Wiley, I. A. Wilson, J. J. Skehel, *ibid.*, p. 373.
31. D. L. Milligan and D. E. Koshland, Jr., in preparation.
32. H.-P. Biemann and D. E. Koshland, Jr., unpublished results.
33. L. Lee and T. Mizuno, *J. Bacteriol.* **170**, 4769 (1988).
34. Y. Imae *et al.*, *ibid.* **169**, 371 (1987).
35. D. L. Milligan and D. E. Koshland, Jr., *J. Biol. Chem.* **263**, 6268 (1988).
36. B. A. Lynch and D. E. Koshland, Jr., *Proc. Natl. Acad. Sci. U.S.A.*, in press.
37. D. L. Milligan and D. E. Koshland, Jr., *Science*, in press.
38. A. M. Honegger, R. M. Kris, A. Ullrich, J. Schlessinger, *Proc. Natl. Acad. Sci. U.S.A.* **86**, 925 (1989).
39. G. R. Moe, G. E. Bollag, D. E. Koshland, Jr., *ibid.*, p. 5683.
40. D. E. Tronrud, L. F. Ten Eyck, B. W. Matthews, *Acta Crystallogr.* **A53**, 489 (1987).
41. J. P. Priestle, *J. Appl. Crystallogr.* **21**, 572 (1988).
42. W. Kabsch and C. Sander, *Biopolymers* **22**, 2577 (1983).
43. Abbreviations for the amino acid residues are: G, Gly; K, Lys; M, Met; N, Asn; Q, Gln; S, Ser; and T, Thr.
44. We thank N. Sakabe, A. Nakagawa, and N. Watanabe of the National Laboratory of High Energy Physics, Tsukuba, Japan, and J. Farrar of Molecular Structure Corp., the Woodlands, Texas, for use of their data collection facilities. G.G.P. thanks the American Cancer Society, California Division, for a postdoctoral fellowship (J-15-89). Supported in part by NIH grants AI 30725 to S.H.K. and DK09765 to D.E.K., DOE (Director, Office of Energy Research, Office of Biological and Environmental Research, General Life Sciences Division under contract DE-AC03-76SF0098 to S.H.K.), and the William M. Keck Foundation. Atomic coordinates will be deposited with the Brookhaven Protein Data Bank.

19 August 1991; accepted 21 October 1991

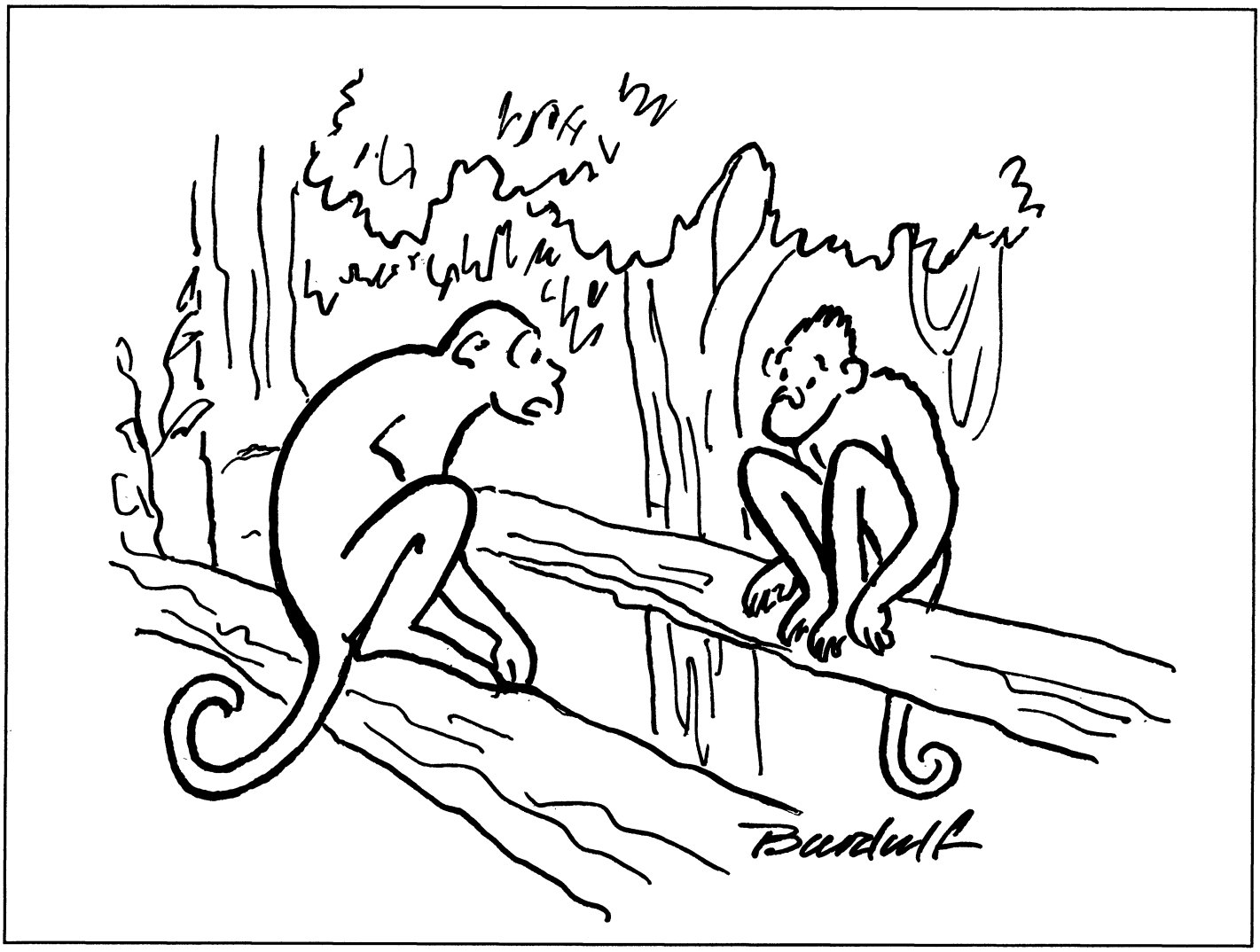

"Of course, I'd like to evolve into something better, but what could that possibly be?"